Fermi National Accelerator Laboratory

FERMILAB-Pub-92/134-A

May, 1992

N-point correlation functions in the CfA and SSRS redshift distribution of galaxies

ENRIQUE GAZTAÑAGA

NASA/Fermilab Astrophysics Center,

Fermi National Accelerator Laboratory, Batavia, IL60510-0500, USA

ABSTRACT

Using counts-in-cells, we estimate the volume-average N-point galaxy correlation functions $\bar{\xi}_N(R)$ for $N = 2, 3$ and 4, in redshift samples of the CfA and SSRS catalogs. Volume limited samples of different sizes are used to study the uncertainties at different scales, the shot noise and the problem with the boundaries.

For each sample, a power-law is obtained for the density contrast in a spherical cell of radius R: $\bar{\xi}_2(R) = (R_0/R)^\gamma$ in agreement with previous estimations. For higher order correlations we found in all samples a good agreement with the hierarchical symmetry: $\bar{\xi}_N = S_N\, \bar{\xi}_2^{N-1}$, for all radius inspected: i.e. from $2 - 22$ Mpc, which included both mildly linear, $\bar{\xi}_2 > 1$, and non-linear, $\bar{\xi}_2 < 1$ scales. The hierarchical constants S_3 and S_4 agree well in all samples in CfA and SSRS with average: $S_3 = 1.94 \pm 0.07$ and $S_4 = 4.56 \pm 0.53$. We compare these results with estimates obtained from angular catalogs and recent analysis over IRAS samples. S_3 and S_4 are larger in real space than in redshift space and smaller for IRAS than for optical galaxies. This observation indicates that the density fluctuations of IRAS galaxies can not be simply proportional to the density fluctuations of optical galaxies, i.e. biasing has to be non-linear between them.

Operated by Universities Research Association Inc. under contract with the United States Department of Energy

1 Introduction

An important test for possible scenarios of galaxy formation is the analysis of the statistical properties of the large scale density distribution of galaxies. One such property is the two-point correlation function $\xi_2(r)$, which has been derived from galaxy catalogs and appears to agree with a power-law:

$$\xi_2(r) = (r_0/r)^\gamma, \tag{1}$$

both in real and redshift space (e.g. Groth & Peebles 1977, Davis & Peebles 1983). Although $\xi_2(r)$ imposes a necessary condition to be satisfied by models, it is not sufficient. Mathematically, the statistical properties can be characterized by the J-point (irreducible) correlation functions, $\xi_J(r_1, ..., r_J)$, for $J = 2, 3, 4....$ The two-point correlation function, $\xi_2(r) \equiv \xi_2(|r_2 - r_1|) = \xi_2(r_1, r_2)$, corresponds to one degree of freedom and, in general, the higher-order correlations are independent. For the galaxy distribution, it has been proposed that the J-point correlation function could be expressed as

$$\xi_J(r_1, ..., r_J) = Q_J \sum_{\{ij\}} [\xi_2(r_{ij})]^{J-1}, \qquad J = 3, 4, 5 \ldots \tag{2}$$

Here the product of the two-point functions, $\xi_2(r_{ij})$, is over $J-1$ independent pairs of relative separations and the sum, consisting of J^{J-2} terms, is over equivalent reassignments of labels $i, j = 1, 2, 3 \ldots, J$. The numbers Q_J might be different for different graphs connecting the labels, and in this case we should introduce a 'topological' dependence: $Q_{N,\alpha}$ where α denotes different topologies in the graphs. A weaker proposal, which includes properties of the hierarchy (2) and the power-law (1), is the scale-invariant symmetry:

$$\xi_J(\lambda r_1, ..., \lambda r_J) = \lambda^{-\gamma(J-1)} \xi_J(r_1, ..., r_J). \tag{3}$$

The above equalities are supported, for $J = 3$ and $J = 4$, by analysis of angular catalogs of optically selected galaxies (Groth and Peebles 1977; Davis and Peebles 1977; Fry and Peebles 1978), on mildly non-linear scales, $\xi_2 > 1$, i.e. from 0.1 up to few Mpc. Similar hierarchical forms have been found for the matter distribution both in perturbation theory with initial gaussian fluctuations (Peebles 1980, Fry 1984b, Juszkiewicz and Bouchet 1991) and in the highly non-linear regime of gravitational clustering (David and Peebles 1977, Fry 1984a, Hamilton 1988, Balian and Schaeffer 1989a and 1989b).

We are going to center our analysis in the the volume-average correlation functions

$$\bar{\xi}_J(V) = \frac{1}{V^J} \int_V d^3r_1 ... d^3r_J \xi_J(r_1, ..., r_J), \tag{4}$$

for which, from equations (3) and (1), a similar hierarchy follows:

$$\bar{\xi}_J(V) = S_J \, [\bar{\xi}_2(V)]^{J-1}. \tag{5}$$

The constants S_J depend only on the shape of the cell and the slope of the two-point correlation function, γ, in equation (1), but not in the size of the cell. Equation (5) also follows directly from the hierarchy (2), with the values of Q_J related to S_J/J^{J-2} by a constant factor, a function of γ which is close to one (see Balian and Schaeffer 1989a). Notice that $S_J = J^{J-2} Q_J$ is usually assumed or used as a definition of Q_J, which could be misleading.

Recent analysis, by Meiksin et al (1991), of angular catalogs of IRAS galaxies suggest that these scaling properties are also valid for the distribution of infrared selected galaxies, though the hierarchical constants Q_J are smaller than the ones for optical galaxies. Bouchet et al. (1991) found similar properties

in *redshift* samples of the IRAS galaxies, again with smaller values of Q_J than in previous results. It is important to check if these are general properties, valid also in redshift samples of optically selected galaxies. To do this, we have studied and compare $\overline{\xi}_J$ for $J = 2, 3$ and 4 in samples of the CfA and the SSRS redshift catalogs.

Throughout the paper we take $h = 1$, where the Hubble parameter $H_0 = 100h$km/sec/Mpc. Dependence on h is readily recovered by putting h^{-1} before the unit of Mpc.

2 Counts-in-cells and correlation functions

The correlation functions are related to counts-in-cells, the probability $P_i(V)$ to find i galaxies in a randomly selected cell of volume V. In our analysis we have estimated the average correlations $\overline{\xi}_J$ from the moments of counts-in-cells, $< i^J > \equiv \sum_i i^J P_i(V)$, using (i.e., Peebles 1980, Fry 1985):

$$\begin{aligned} < i > &= \overline{N} \\ < (\Delta i)^2 > &= \overline{N}^2\overline{\xi}_2 + \overline{N} \\ < (\Delta i)^3 > &= \overline{N}^3\overline{\xi}_3 + 3\overline{N}^2\overline{\xi}_2 + \overline{N} \\ < (\Delta i)^4 > -3 < (\Delta i)^2 >^2 &= \overline{N}^4\overline{\xi}_4 + 6\overline{N}^3\overline{\xi}_3 + 7\overline{N}^2\overline{\xi}_2 + \overline{N} \end{aligned} \tag{6}$$

where $\Delta i \equiv i - < i >$. Notice that $P_i(V)$ is a function of the volume of the cell, V, where $\overline{\xi}_J(V)$ is averaged.

We estimate $P_i(V)$ in the following way. Given the radius R of a test-sphere, we choose randomly its center inside the survey sample, count the number of galaxies found inside the cell and accumulate the number of cells N_i with $i = 0, 1, 2, 3...$ galaxies. We repeat the procedure many times so that the sampling spheres overlap with each other. The coverage c, the frequency each galaxy is covered by a test-cell on average, is related to the total number of independent cells: $N_c = cV_t/V$, with V_t the total volume of the sample. The maximum value of c is constrained by how much the galaxies are correlated. Gaztañaga and Yokoyama (1992) found an upper bound $c \lesssim \overline{\xi}_2^{-3/2}$, which will determine the size of the error-bars in our analysis. Counts-in-cells are estimated by $P_i = N_i/N_c$, the precision or error is limited by the number of independent cells sampled N_c, i.e. from the binomial distribution: $\delta P_i/P_i > (P_i N_c)^{-1/2}$, for $P_i \ll 1$.

3 Analysis of the observational data

3.1 Galaxy catalogs

Two different catalogs of galaxies are used. One is the North Zwicky Center for Astrophysics (CfA1) catalog with $m_B < 14.5$, $\delta \geq 0$, and $b^{II} \geq 40°$ which has a solid angle of 1.83sr (Huchra *et al.* 1983). The other is the Southern Sky Redshift Survey (SSRS) of diameter-selected galaxies from the ESO catalog with $\delta \leq -17.5°$, $b^{II} \leq -30°$, and the solid angle of 1.75sr (Da Costa *et al.* 1988). Heliocentric redshifts are corrected only from our motion with respect to the rest frame of the Cosmic Microwave Background; $v = 365$km/sec and the direction $(\alpha, \delta) \sim (11.2^h, -7°)$ (Smoot *et al.* 1991).

We select three different volume-limited samples out of each catalog as shown in Table 1, where $v_{\rm lim}$ is the maximum redshift and $N_{\rm tot}$ the total number of galaxies. Samples CfAN80 and CfAN92 include galaxies brighter than $M_B = m_B - 25 - 5\log(v_{\rm lim}/H_0)$, where $m_B = 14.5$ is the limiting apparent magnitude. Sample CfAN50 includes galaxies brighter than $M_B = -19$ but fainter than $M_B = -20$, so

that this sample is independent of CfAN80 or CfAN92. Samples SSRS50, SSRS80 and SSRS115 include galaxies with physical diameter greater than $d_{\rm lim} = v_{\rm lim}\theta_{\rm cut}/H_0$, where $\theta_{\rm cut} = 1'.26$ is the 'face-on' diameter cut-off.

Redshifts smaller than 2500Km/s are not taken into account, since typical peculiar velocity flows (of several hundreds of Km/s) can compete with the general recession velocity.

3.2 Consistency and 2-point correlation functions

For each sample, counts-in-cells are estimated for spherical cells of radius R in a range between $2-22$Mpc as shown in Table 1. The smaller scale in the range of R (in Table 1) is chosen to avoid fluctuations from shot noise, whereas the larger scale is fixed to avoid problems with the boundary. We have compared two prescriptions to deal with the boundary. One is to center the cells so that the entire sphere is contained in the surveyed region. The other is to adopt periodic boundary conditions. The former weights more the central region of the sample whereas the latter compares galaxies which are not physically correlated. We have found that, provided we choose spheres smaller than about 5-10% the total volume in each sample, both prescriptions agree within the errors. For larger scales we found similar systematic effects in all samples: i.e. large statistical errors and quickly diverging correlations. This is interpreted to be consequence of the boundary, as it happens for cells with the same large fraction of the total volume in each sample. Periodic boundary conditions have been used in the analysis presented below because they provide uniform sampling and better signal/noise ratio.

It is checked that the measured counts are normalized, $\sum_i P_i(R) = 1$, within the errors. Furthermore, we have made a consistency test, by calculating the average number of galaxies in a cell $\overline{N} \equiv < i >$ and the fluctuations $< (\Delta i)^2 >$. We expect $\overline{N} = nV$, where n is the density of galaxies in each sample and V the volume of the cell: $V = 4/3\pi R^3$. In practice $\overline{N}$ could deviate from nV for large cells depending on the way the boundary is sampled.

Figures 1 show the average correlation function, $\overline{\xi}_2(R)$, estimated from $< (\Delta i)^2 >$ by equation (6), for the values of R consider in each sample. These correlations agree well with a numerical integration over the cell volume (4) of the two-point correlation function $\xi_2(s)$, obtained directly by counting pairs. In Table 1, we show the correlation length, s_0, and slope, γ, for a redshift correlation function, $\xi_2(s) = (s/s_0)^\gamma$, fitted in the corresponding scales for each sample.[1] An interesting problem is why the samples with smaller volume in each catalog have smaller correlation length s_0 (see Davis et al.1988 and Pellegrini et al. 1990). It might be that these data sets are not yet a 'fair sample' or that there is some real segregation, either with luminosity, volume or location.

3.3 3-point and 4-point correlations

The third and fourth moments of counts-in-cells are used to estimate $\overline{\xi}_3(R)$ and $\overline{\xi}_4(R)$. In Figures 2, $\overline{\xi}_3$ and $\overline{\xi}_4$ are plotted as a function of $\overline{\xi}_2$ for all samples. Table 1 shows the parameters of a fit to: $\overline{\xi}_3 = S_3\overline{\xi}_2^{\eta_3}$, $\overline{\xi}_4 = S_4\overline{\xi}_2^{\eta_4}$. Although the errors are quite big, there is evidence for $\eta_3 = 2$ and $\eta_4 = 3$, following (5). The errors in S_J and η_J are propagated from the errors in P_i, which correspond to a 90% confidence in a student distribution of different realizations of the random sample of test-cells positions. Notice that although samples N50 and SSRS50 have small amplitudes of $\overline{\xi}_2$ they have similar hierarchical pattern than the other samples.

[1] For some samples, the values of s_0 and γ are quite sensible to the range of scales chosen to do the fit.

The average of the mean values of $\bar{\xi}_J/\bar{\xi}_2^{J-1}$ for all scales and samples are: $S_3 = 1.94 \pm 0.07$ and $S_4 = 4.56 \pm 0.53$; with a 95% interval of confidence. There is a small difference for S_3 and S_4 between the corresponding averages in the SSRS and CfA as shown in Table 2. Estimates and models for S_3 and S_4 are summarized in Table 2. When only Q_3 or Q_4 are available we used, in parenthesis, $S_3 \simeq 3Q_3$ and $S_4 \simeq 16Q_4$, as the error induced by this approximation is comparable with the errors of Q_3 and Q_4. Besides the method explained in this paper, based on $\bar{\xi}_J(V)$, a direct count of triplets and quadruples in angular space, $\omega_J(\theta_1, .., \theta_J)$, have been used by Groth and Peebles (1977) and Fry and Peebles (1978); whereas moments of angular counts, $\omega_{mn}(\theta)$, has been used by Meiksin et al. (1991). Observational results based on angular catalogs, are labeled by ϕ, the selection function. Both Fry's (1984a) and Hamilton (1988) BBGKY models agree with our estimates of S_4 once we fix $S_3 = 3Q$, a free parameter in these models. Schaeffer's (1984) parametrization fits our data for $\nu \simeq -1.6$.

4 Conclusion

The volume-average correlations: $\bar{\xi}_2(R)$, $\bar{\xi}_3(R)$ and $\bar{\xi}_4(R)$ are estimated for spheres of radius R between $2 - 22$Mpc. We found that $\bar{\xi}_2(R)$ behaves like a power-law (Figures 1), and that both $\bar{\xi}_3(R)$ and $\bar{\xi}_4(R)$ follow the hierarchy $\bar{\xi}_J = S_J\, \bar{\xi}_2^{J-1}$, with averages $S_3 = 1.94 \pm 0.07$ and $S_4 = 4.56 \pm 0.53$ (Figures 2), for $7 > \bar{\xi}_2 > 0.1$, including mildly linear ($\xi_2 < 1$) and non-linear ($\xi_2 > 1$) scales. The errors in each sample are too big to detect the dependence of S_3 and S_4 on the slope of $\bar{\xi}_2$ (i.e. γ in Table 1), which is expected from the hierarchical properties (2) or (3). Further work should consider cells of different shapes (i.e. Elizalde and Gaztañaga 1992) to study other aspects of the multi-point hierarchy (3) and (2).

The analysis presented here is over redshift space and not over real space. The comparison of S_3 and S_4 from different catalogs in Table 2 shows that, for both infrared and optically selected samples, the values in the redshift distribution are smaller than the corresponding values in angular catalogs, i.e. real space, in qualitative agreement with the CDM simulations by Lahav et. al (1992). The CfA and SSRS redshift surveys have slightly larger values of S_3 and similar values of S_4 than the IRAS redshift survey analyzed by Bouchet et al. (1991). This is to be contrasted with the results by Meiksin et al. (1991) which suggest a larger difference between optical and IRAS distributions in real space. It should be noticed though, that the values calculated from the angular analysis correspond to smaller scales, where we might expect large non-perturbative effects and more important redshift distortions (see Lahav et al. 1992).

To compare these results with theoretical estimates, for example with perturbation theory, one has to address both the problem of the distortions of the redshift distribution and the problem of the relation between galaxy and matter distribution. In general, the galaxy (redshift) distribution might have different statistical properties than the matter distribution. The standard biasing assumption is that δ_{rms} for the galaxy distribution is proportional to $\delta_{\rm rms}^{(m)}$ for the matter distribution, i.e. $\delta_{\rm rms} = b\, \delta_{\rm rms}^{(m)}$. A stronger assumption, called *linear biasing*, is that the galaxy fluctuation δ, rather than $\delta_{\rm rms} \equiv < \delta^2 >^{1/2}$, is proportional to the matter fluctuation: $\delta = b\, \delta^{(m)}$. Linear biasing predicts that a hierarchical matter distribution with constants $S_J^{(m)}$ would generate a hierarchical galaxy distribution with different hierarchical constants, i.e. using (5) we have $S_J = b^{-J+2}\, S_J^{(m)}$. However, not both IRAS and optical galaxies can have density fluctuations proportional to matter fluctuations. In other words, there can not be a linear biasing between optical (O) and IRAS (I) distributions. This can be seen in Table 2, where for both redshift and real space: $S_3^I < S_3^O$, which for linear biasing implies: $b^I/b^O = S_3^O/S_3^I > 1$, in contradiction with the observed value $b^I/b^O \simeq 0.69 \pm 0.09$ (Saunders et al. 1992).

If the hierarchical properties observed correspond to the matter distribution, the results of perturbational analysis (see Peebles 1980, Fry 1984b, Bouchet et al. 1991 and Juszkiewicz and Bouchet 1991) could indicate that the distribution we observed is a consequence of gravitational evolution from initially gaussian fluctuations, with $S_3^{(m)} = 34/7 - (n+3)$ (Juszkiewicz and Bouchet 1991). A linear biasing for the samples in our analysis, i.e. $S_3 = S_3^{(m)}/b = 1.94 \pm 0.07$, yields $b = 1.47 \pm 0.05$ for a $n = -1$ initial power spectrum.

In order to assess the necessity of such interpretation we need to understand better galaxy-matter biasing, redshift distortions and perturbation analysis from non-gaussian initial conditions.

Acknowledgements

I am grateful to Jun'ichi Yokoyama for his counceling and L.N. Da Costa who provide the SSRS data. This work was supported in part by DOE and NASA (grant NAGW-2381) at Fermilab and by Fulbright/MEC (grant FU91 14594408).

References

Balian, R. and Schaeffer, R. 1989a, *Astr. Astrophys.*, **220**, 1.
Balian, R. and Schaeffer, R. 1989b, *Astr. Astrophys.*, **226**, 373.
Bouchet, F.R., Davis, M. and Strauss M. 1991, *Proceedings DAEC Workshop* (Editor: G.Mamon).
Da Costa, L.N. *et al.* 1988, *Ap.J.*, **327**, 544.
Davis, M. and Peebles, P.J.E. 1977, *Ap.J. Suppl.*, **35**, 425.
Davis, M. and Peebles, P.J.E. 1983, *Ap.J.*, **267**, 465.
Davis, M.. Meiksin, A., Strauss, M.A., da Costa, L.N. and Yahil, A. 1988, *Ap.J.(Letters)*, **333**, L9.
Elizalde, E. and Gaztañaga, E. 1992, *M.N.R.A.S*, **254**, 247.
Fry, J.N. and Peebles, P.J.E. 1978, *Ap.J.*, **221**, 19.
Fry, J.N. 1984a, *Ap.J.*, **277**, L5.
Fry, J.N. 1984b, *Ap.J.*, **279**, 499.
Fry, J.N. 1985, *Ap.J.*, **289**, 10.
Gaztañaga, E. and Yokoyama, J 1992, FERMILAB-Pub-92/71-A.
Groth, E.J. and Peebles, P.J.E. 1977, *Ap.J.*, **217**, 385.
Hamilton, A.J.S. 1988, *Ap.J.(Letters)*, **332**, 67.
Huchra, J., Davis, M., Latham, D., and Tonry, J. 1983, *Ap.J. Suppl*, **52**, 89.
Lahav, O., Itoh, M, Inagaki, S. and Suto Y. 1992, Submited to Ap.J.
Juszkiewicz, R. and Bouchet 1991, *Proceedings DAEC Workshop* (Editor: G.Mamon).
Meiksin, A., Szapudi, I. and Szalay, A.S. 1991, John Hopkins University preprint 100.
Peebles, P.J.E. 1980, *The Large-Scale Structure of the Universe* (Princeton University Press: Princeton).
Pellegrini, P.S., Willmer, C.N.A., da Costa, L.N. and Santiago, B.X. 1990, *Ap.J.*, **350**, 95.
Saunders, W., Rowan-Robinson M. and Lawrence A. 1992, to be published in M.N.R.A.S.
Schaeffer, R. 1984, *Astr. Astrophys. Lett.*, **134**, L15.
Smoot, G.F. *et al.* 1991, *Ap.J.(Letters)*, **371**, L1.

Figure Captions

Figures 1. Average correlation function, $\bar{\xi}_2(R)$, for different spherical cells of radius R in each sample. The filled circles, opened circles and filled squares correspond to CfAN50, CfAN80 and CfAN92 for the CfA and to SSRS50, SSRS80 and SSRS115 for the SSRS. The dashed line correspond ro $\bar{\xi}_2(R) \propto R^{-1.8}$.

Figures 2. Values of $\bar{\xi}_J(R)$ as a function of $\bar{\xi}_2(R)$: Fig. 2a shows $\bar{\xi}_3(R)$ and Fig. 2b shows $\bar{\xi}_4(R)$. Open triangles, circles and squares correspond to CfAN50, CfAN80 and CfAN92 whereas filled triangles, circles and squares correspond to SSRS50, SSRS80 and SSRS115. The dashed lines are the hierarchical law: $\bar{\xi}_J = S_J \bar{\xi}_2^{J-1}$ with $S_3 = 1.94$ and $S_4 = 4.56$.

Tables

Table 1: Galaxy samples.

Sample	CfAN50	CfAN80	CfAN92	SSRS50	SSRS80	SSRS115
$v_{\rm lim}$ (Km/s)	5000	8000	9200	5000	8000	11500
$M_B/d_{\rm lim}$	[−19,−20]	< −20.0	< −20.3	> 18.3 Kpc	> 29.2Kpc	> 42.0Kpc
$N_{\rm tot}$	191	214	146	243	220	134
Volume (Mpc^3)	6.7×10^4	3.0×10^5	4.7×10^5	6.4×10^4	2.9×10^5	8.8×10^5
Spiral (%)	72	52	55	78	80	83
Range of R (Mpc)	2-8	4-12	8-22	2-8	4-12	8-22
$s_0 \pm 1$	4 Mpc	8 Mpc	7 Mpc	5 Mpc	7 Mpc	8 Mpc
$\gamma \pm .1$	1.8	1.5	1.7	1.4	1.3	1.8
$S_3 = \overline{\xi}_3/\overline{\xi}_2^{\eta_3}$	1.74 ± 0.28	1.71 ± 0.23	$1.66 \pm .52$	1.40 ± 0.54	1.93 ± 0.35	$2.22 \pm .86$
η_3	2.03 ± 0.26	2.16 ± 0.21	1.87 ± 0.30	2.29 ± 0.40	2.05 ± 0.25	1.99 ± 0.38
$S_4 = \overline{\xi}_4/\overline{\xi}_2^{\eta_4}$	3.3 ± 1.5	2.5 ± 1.1	3.0 ± 4.3	1.7 ± 2.3	4.4 ± 2.0	6.6 ± 8.5
η_4	3.0 ± 0.7	3.8 ± 1.0	2.8 ± 1.1	3.9 ± 1.1	3.1 ± 0.5	3.3 ± 0.8

Table 2: Estimates and models for S_3 and S_4.

$S_3(3Q_3)$	$S_4(16Q_4)$	Sample/Model	Method/Parameter	Reference
(3.87 ± 0.63)	—	LICK-Zwicky	$\omega_J(\theta_1,..,\theta_J);\phi$	Groth & Peebles 1977
—	(46 ± 8)	LICK-Zwicky	$\omega_J(\theta_1,..;\theta_J);\phi$	Fry & Peebles 1978
(4.32 ± 0.21)	(31 ± 5)	LICK	$\omega_{nm}(\theta);\phi$	Meiksin et.al 1991
(2.19 ± 0.18)	(10.1 ± 2.9)	IRAS	$\omega_{nm}(\theta);\phi$	Meiksin et.al 1991
(2.40 ± 0.21)	—	CfA	$\omega_J(\theta_1,..,\theta_J);\phi$	Peebles 1980
1.5 ± 0.5	4.4 ± 3.7	IRAS (redshift)	$\overline{\xi}_J(V)$	Bouchet et.al 1991
1.86 ± 0.07	4.15 ± 0.60	CfA (redshift)	$\overline{\xi}_J(V)$	This paper
2.01 ± 0.13	4.96 ± 0.88	SSRS (redshift)	$\overline{\xi}_J(V)$	This paper
$3(4/3)^\nu$	$2^{4+\nu}$	Parametric	ν	Schaeffer 1984
$3Q$	$32/3Q^2$	BBGKY aprox.	Q	Fry 1984a
$3Q$	$12Q^2$	BBGKY aprox.	Q	Hamilton 1988
2	6	Negative binomial	Non	Fry 1985
$34/7-(n+3)$	—	perturbation	n-initial power	Juszkiewicz & Bouchet 1991

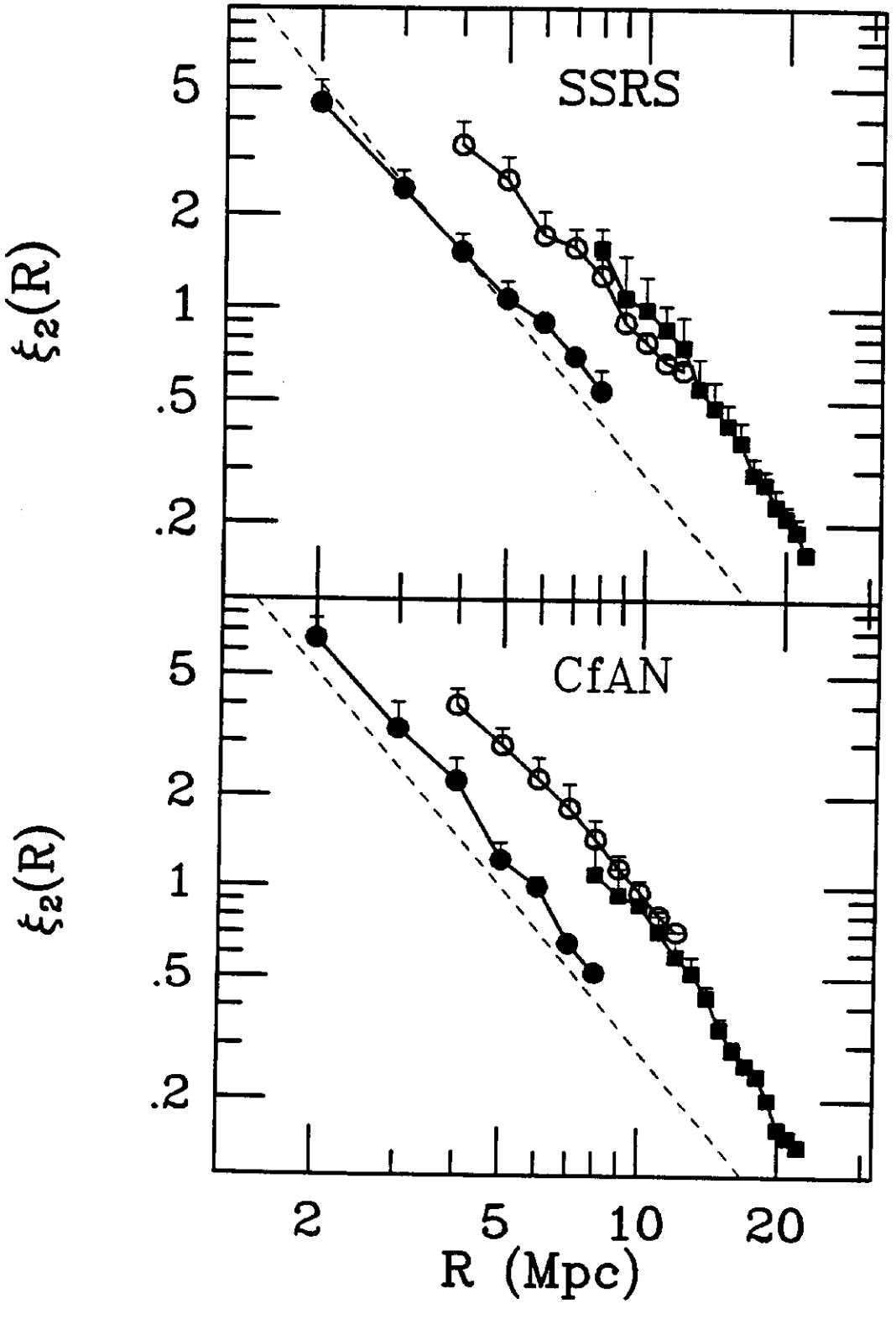

Fig. 1

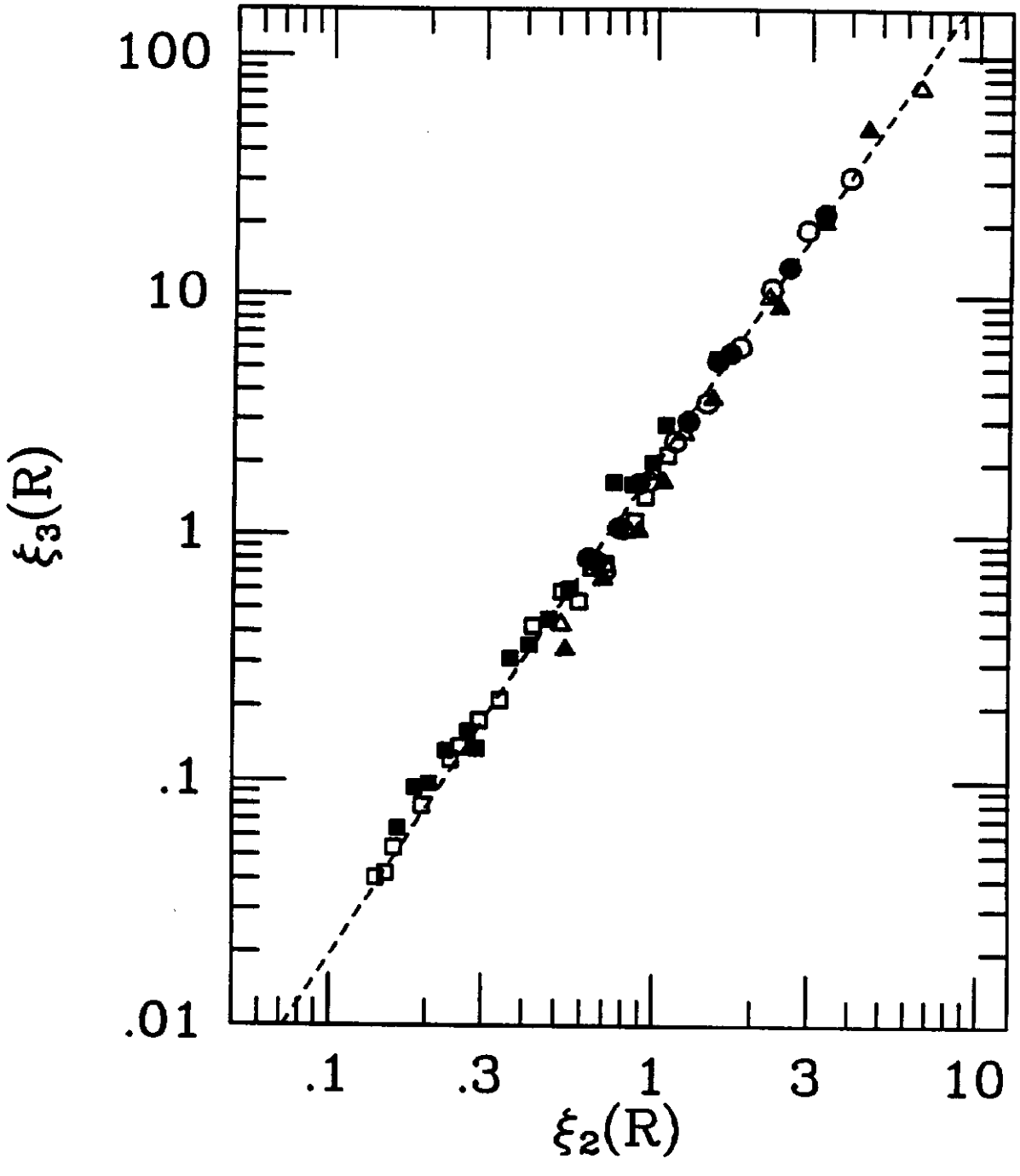

Fig 2a.

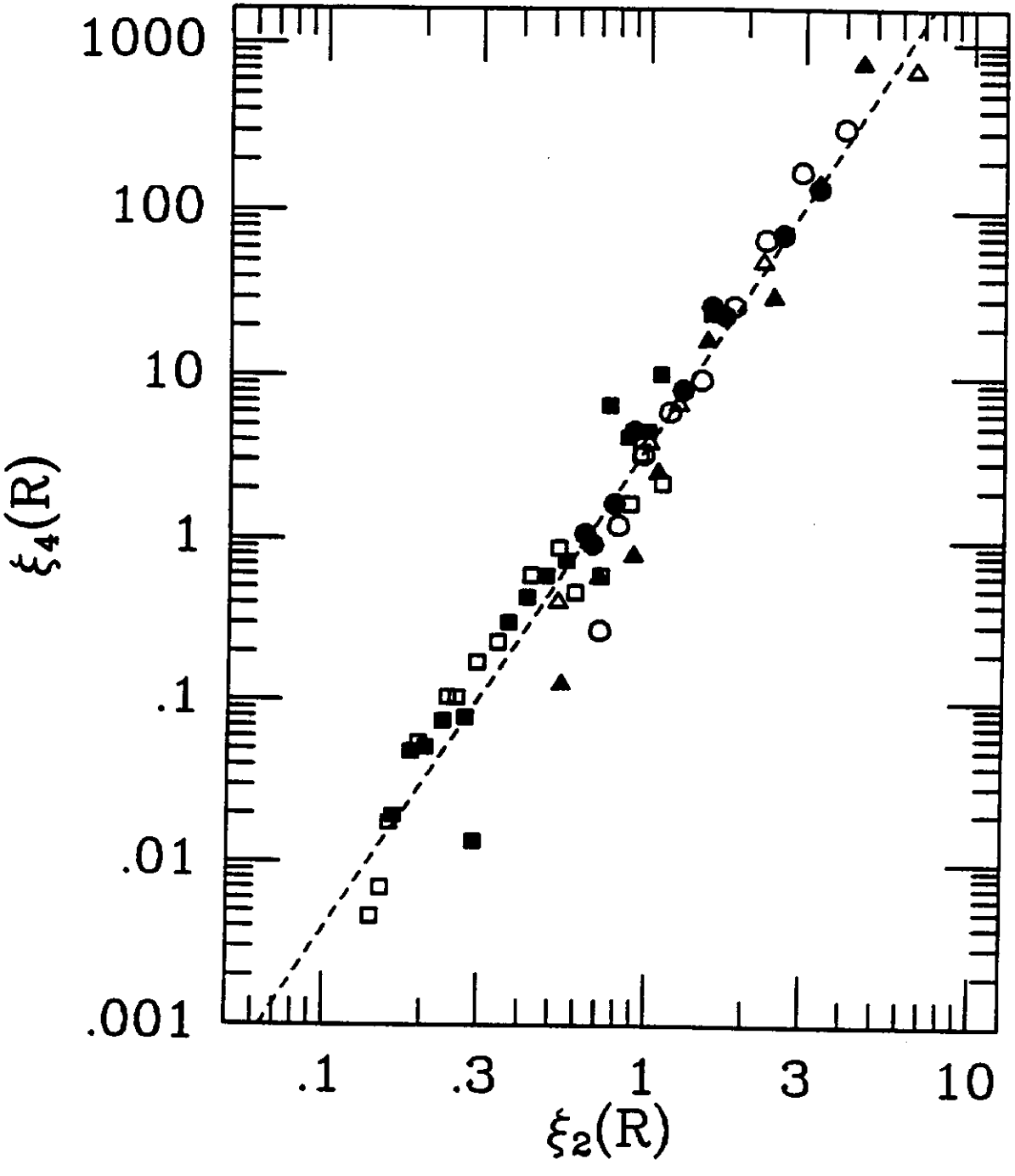

Fig 2b